Separation Science and Technology
Publication details, including instructions for authors and subscription information:
http://www.informaworld.com/smpp/title~content=t713708471

Morphology of Sludge Cake at Electroosmosis Dewatering

C. P. Chu[a]; D. J. Lee[a]; Z. Liu[b]; W. H. Jin[b]
[a] Department of Chemical Engineering, National Taiwan University, Taipei, Taiwan [b] Department of Chemical Engineering, Tsinghua University, Beijing, China

Online publication date: 08 July 2010

To cite this Article Chu, C. P. , Lee, D. J. , Liu, Z. and Jin, W. H.(2005) 'Morphology of Sludge Cake at Electroosmosis Dewatering', Separation Science and Technology, 39: 6, 1331 — 1346
To link to this Article: DOI: 10.1081/SS-120030486
URL: http://dx.doi.org/10.1081/SS-120030486

SEPARATION SCIENCE AND TECHNOLOGY
Vol. 39, No. 6, pp. 1331–1346, 2004

Morphology of Sludge Cake at Electroosmosis Dewatering

C. P. Chu,[1] D. J. Lee,[1,*] Z. Liu,[2] and W. H. Jin[2]

[1]Department of Chemical Engineering, National Taiwan University, Taipei, Taiwan
[2]Department of Chemical Engineering, Tsinghua University, Beijing, China

ABSTRACT

Sludge cakes sampled at various positions and times in an electroosmosis-dewatering chamber were analyzed using microtome-slicing techniques. The flocs accumulated at the anode due to the electrostatic attraction. The porosity continued to decrease as most of the biomass coagulated into large clusters. During the constant-rate period of moisture removal, the morphological differences between the cakes at the two electrodes were less significant. During the falling-rate period, a relatively large difference in cake porosity appeared between the electrodes, involving

*Correspondence: D. J. Lee, Department of Chemical Engineering, National Taiwan University, Taipei, Taiwan 10617; Fax: +886-2-2362-3040; E-mail: djlee@ccms.ntu.edu.tw.

DOI: 10.1081/SS-120030486 0149-6395 (Print); 1520-5754 (Online)

difference in pore size, porosity, Sierpinski fractal dimension (D_{SC}), and pore boundary fractal dimensions (D_B).

Key Words: Sludge cakes; Electroosmotic dewatering; Microtome; Pore.

INTRODUCTION

Electroosmotic dewatering has been proposed to be effective in the solid–liquid separation of hard-filtered slurries. Combining electroosmotic dewatering with pressure filtration can improve dewatering performance over that of conventional dewatering devices. Several prototype pilot plants that employ mechanical-electroosmotic dewatering apparatus have been reportedly used for commercial applications.[1–3] Surface charges on particulate materials dominate dewatering performance. Changing the ζ potential of flocs by adjusting their pH and ionic strength, or by chemical conditioning, was studied for its potential to facilitate dewatering.[4,5] Zhou et al.[6] further considered the effects of several physical conditioning procedures on sludge, including thermal treatment and freezing/thawing.

The structure of the cake may also be an essential factor in determining the efficiency of electroosmotic dewatering. Laursen and Birgerjensen[7] presented a picture of the structural change of the filter cake during electroosmotic dewatering. Kondoh and Hiraoka[1] compared SEM microphotographs of sludge cakes at the anode and cathode. Microbial substances, which often clog the filter, accumulated near the anode, while the cake at the cathode-side was comprised mainly of silt and fibrous matter. Yoshida et al.[8,9] found that as the moisture was extracted during electroosmosis, water films ceased to be continuous in pores, and the conductivity, electrode contact resistance and electrical potential distribution changed accordingly. Weber and Stahl[10] also stated that the generated bubbles decreased the saturation of the cake and increased the electrical resistance between the two electrodes. Zhou et al.[6] also compared SEM pictures of cakes obtained by electroosmotic dewatering in a horizontal electrical field and those by vacuum filtration. The homogeneity of electroosmotically-dewatered cake implied that most capillary water in the cake was effectively removed.

Most studies qualitatively described sludge cakes subjected to electroosmotic dewatering. Quantitative analyses of cake structures, including porosity and pore size and shape, which should correlate with the electroosmotic dewatering efficiency, are still lacking. This report examines the temporal and spatial structural evolution of sludge cake dewatered in a horizontal electrical field. Microtome slicing and image analysis were performed to

analyze the cake at the anode, at the cathode, and in the middle compartment of the filter, respectively. The porosity, pore size, and morphological fractal dimensions were subsequently determined.

EXPERIMENTAL

Sludge Samples

Sludge was sampled from the sediment in a secondary anaerobic digester at the Gaobeidian wastewater treatment plant, Beijing. It was black in appearance and had a bad odor. After it was gravitationally thickened, its total solid content (TS) reached 4.19% (w/w), and the thickened samples were used in subsequent dewatering tests. The pH value was 8.2, and the conductivity at 25°C was 5000 μS/cm. The volume-average floc size was 15.9 μm and the ζ potential was −22.4 mV. Figure 1 displays a microscopic photograph of the sludge flocs.

Dewatering Apparatus

Figure 2 presented the electroosmotic dewatering apparatus in a horizontal electrical field. It was opened to the atmosphere and there was no pressure

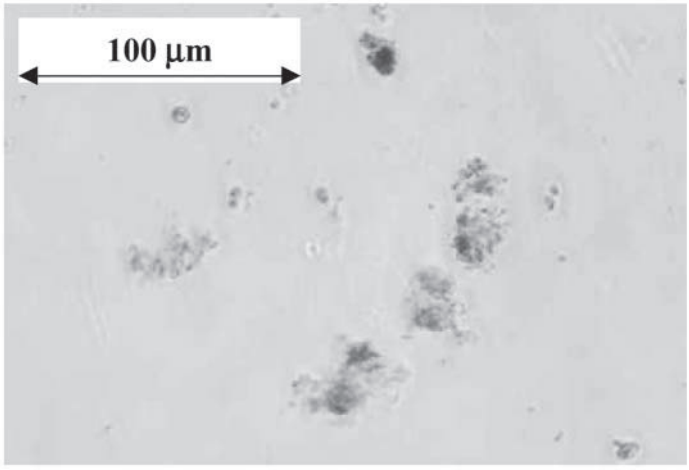

Figure 1. The phase-contrast microphotograph of sludge flocs (400×).

MARCEL DEKKER, INC.
270 Madison Avenue, New York, New York 10016

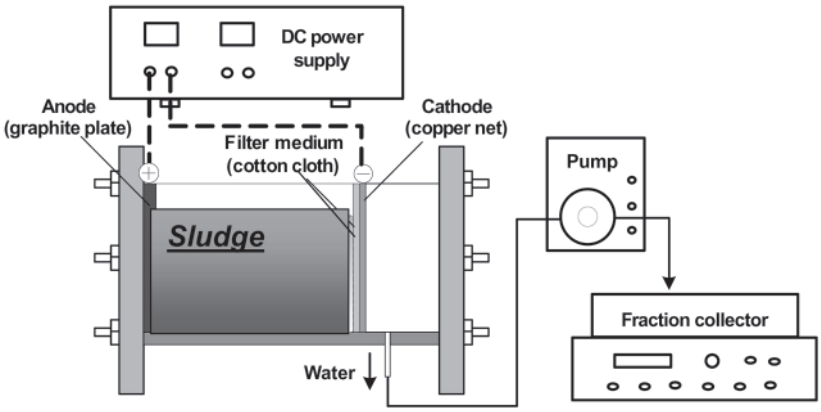

Figure 2. Electroosmotic dewatering apparatus with horizontal electrical field.

difference between the two electrodes. A carbon graphite plate was used as the anode and a copper net was used as the cathode. The cathode was covered with cotton cloth as a filter medium. The cross-sectional area of the loading compartment was 85 mm × 42 mm and the distance between the two electrodes was 65 mm. A variable-DC power supply was used as electrical generator. The applied voltage was set as 50 V. The fluid filtered was removed by a variable-speed tubing pump. A continuous sampler collected the filtrate to yield the time evolution of moisture removal. More details of this device are available in Ref.[6]. The electrodewatering process was performed for 3 hr.

Microtome Slicing

The samples were first chemically fixed using a formalin buffer at 4°C for 24 hr and embedded by agarose in the cassette. Dehydration was conducted by immersing the cake subsequently in ethanol/water solution of 50%, 70%, 90%, 95%, and 100% (v/v), respectively. The ethanol was then replaced by xylene/ethanol solutions of 50%, 70%, 90%, 95%, and 100% (v/v). The cake saturated with xylene was immersed in molten paraffin at 65°C overnight. Finally the paraffin-embedded cakes were cooled to 25°C in peel-off molds and solidified to form blocks for slicing.[11] The block was then sliced into sections of thickness 5 μm using a microtome (Leitz Model 1400, Germany). The thin paraffin section was floated on a water bath and then transferred onto a glass slide. The slide was dried in air. Then, the slice was heated

in an oven at 70°C for 10 min to melt the paraffin, before being dewaxed using xylene. Finally, the slice was stained using hematoxylin and eosin (H&E).[12] A phase-contrast microscope (LEICA DME, Germany) and a digital camera (NIKON COOLPIX 995, Japan) recorded the image of slices at a constant luminescence light (4000 Lux).

Image Processing

Sliced images in red–green–blue (RGB) mode are first converted to grayscale images to construct a histogram of pixels vs. luminescence intensity by *INSPECTOR* (Matrox, Canada). A region of interest (ROI) was defined on the sliced image to include sufficient morphological detail for analysis and to avoid the inhomogeneity of the luminescent background. A larger ROI is required to analyze the filter cake structure, since interstices among the aggregates in the cake may be possibly larger than 100 μm. In this report, the microphotograph with a magnification of 40× (1097 μm at its side, 0.71 μm/pixel) was used to analyze the cake structure. The characteristic length L of ROI was set to 500 μm (approximately 700 pixels) and was much larger than most flocs or pores in the filter cake.

Morphological information extracted from sliced images depends on the image thresholding value. Chu[13] commented that the Otsu's method (detail in Appendix) yielded satisfactory thresholding among the histogram-based algorithms and was chosen herein to estimate the cake porosity. The maximum convex perimeter method was adopted to probe the shapes and spatial distribution of the pores among the biomass granules (detail also in the Appendix).

RESULTS AND DISCUSSION

Dewatering Performance

Figure 3 plots the moisture removal curves of sludge during electroosmotic dewatering. The moisture content in the sludge declined from an initial value of 23 kg/kg DS (95.8%, w/w) to 12 kg/kg DS (92.3%, w/w) at the end of the tests [Fig. 3(a)]. The dewatering rate initially increased from 0.87 g/kg DS/sec to the maximum of 1.20 g/kg DS/sec after 70 min, and then dropped, reaching a final value of 0.69 g/kg DS/sec [Fig. 3(b)]. In the final stage of the tests, the dewatering rate decreased greatly but remained above zero (the 180th minute). The application of electric field leads to the electrolysis of water at two electrodes, which contributes to an acidic pH in anode

Marcel Dekker, Inc.
270 Madison Avenue, New York, New York 10016

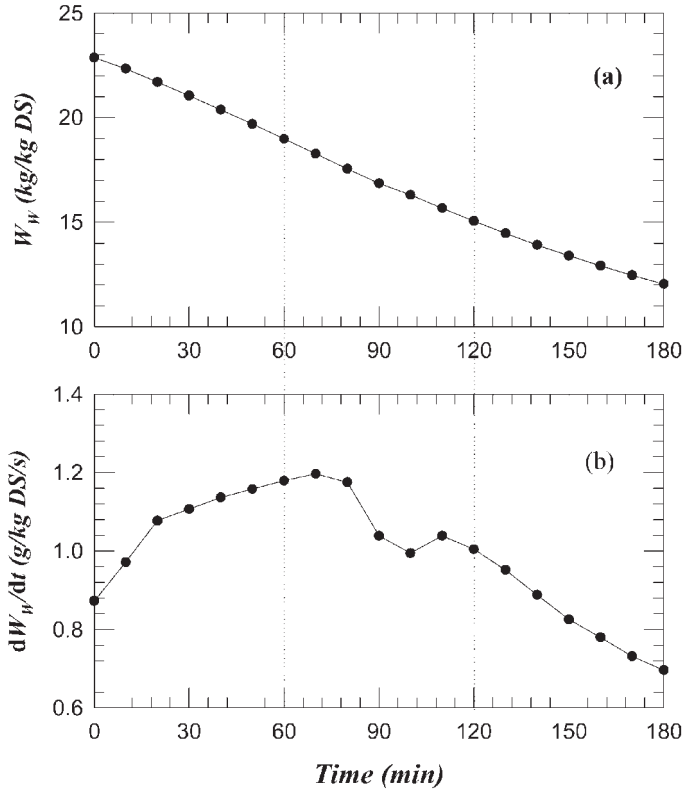

Figure 3. The dewatering rate of sludge: (a) the remained moisture in the cake; (b) the moisture removal rate.

while an alkaline pH in cathode, respectively. At the beginning of the process, the OH^- generated at cathode was first carried out by electroosmotic flux, which caused the increase of pH and decrease of electroconductivity of collected liquid at cathode. This helped to increase the moisture removal rate. With the development of electrodewatering process, the alkaline pH near cathode will be neutralized by H^+ flux from anode and increase the electroconductivity. So the moisture removal rate decreased. Similar results were reported by Hamed and Bhadra[14] in their study of electroremediation of contaminated soil. The moisture-removal rate increased to some steady value (the constant-rate period, the 20th–80th minutes in this case) while the liquid film in the cake remained continuous. When most free moisture had been removed, the liquid phase in the cake pores became discontinuous.

MARCEL DEKKER, INC.
270 Madison Avenue, New York, New York 10016

The interstitial and surface water were then extracted at this time (the falling-rate period, the 90th–180th minutes in this case). Meanwhile, the discontinuous moisture distribution in the cake might also have changed the electrokinetic characteristics of the sludge, thereby decreasing the corresponding conductivity, as described by Yoshida et al.[8,9] The morphological characteristics of the cake before dewatering, at the first hour, the second hour, and at the end of the test (the third hour) were analyzed.

Cake Morphology

Figure 4 plots the morphological changes in the sludge cake, from the sludge suspension at the zeroth hour (approximately 4.2%, w/w) to the end of dewatering (after the third hour), at the cathode, in the middle compartment of the filter, and at the anode, respectively. For brevity, only the microphotographs at a magnification of 40× (the length scale labeled on the photographs, 0.71 μm/pixel) are displayed. Only tiny biomass clusters are distributed on the slice, and large interstices were present among these clusters before dewatering (zeroth hour) [Fig. 4(a)]. As dewatering proceeded, larger and more compact biomass clusters appeared, implying that the aggregation of biomass was caused by the electrostatic attraction and the loss of moisture. The pores shrunk slightly to a size equivalent to that of the biomass clusters [the first hour, Fig. 4(b)–(d), and second hour, Fig. 4(e)–(g)]. In the final stage [the third hour, Fig. 4(h)–(j)], the shrinkage of the biomass clusters was clearly noted at the anode and in the middle.

The spatial difference in morphology at different electrodes was less obvious. Roughly, the cakes at the anode were porous, whereas the cakes in the middle and at the cathode were relatively compact. The difference became noticeable in the final stage of dewatering [Fig. 4(h) and 4(j)]. Water was extracted from the filter medium at the cathode and flocs accumulated on the positively charged anode. Some parts of the cake at the anode may have become unsaturated, due to an absence of moisture replenishment, and large pores appeared because of the shrinkage of those partially unsaturated biomass clusters. This phenomenon was not observed near the cathode, where no large pores formed. Weber and Stahl[10] reported that the bubbles generated from the electrolytic decomposition of water at the anode could not escape and displaced the moisture in the suspension. This made the cake no longer saturated and led to the formation of large pores. The electrolytic effects at the cathode may be relatively insignificant, since the bubbles could escape with the filtrate at cathode.

Marcel Dekker, Inc.
270 Madison Avenue, New York, New York 10016

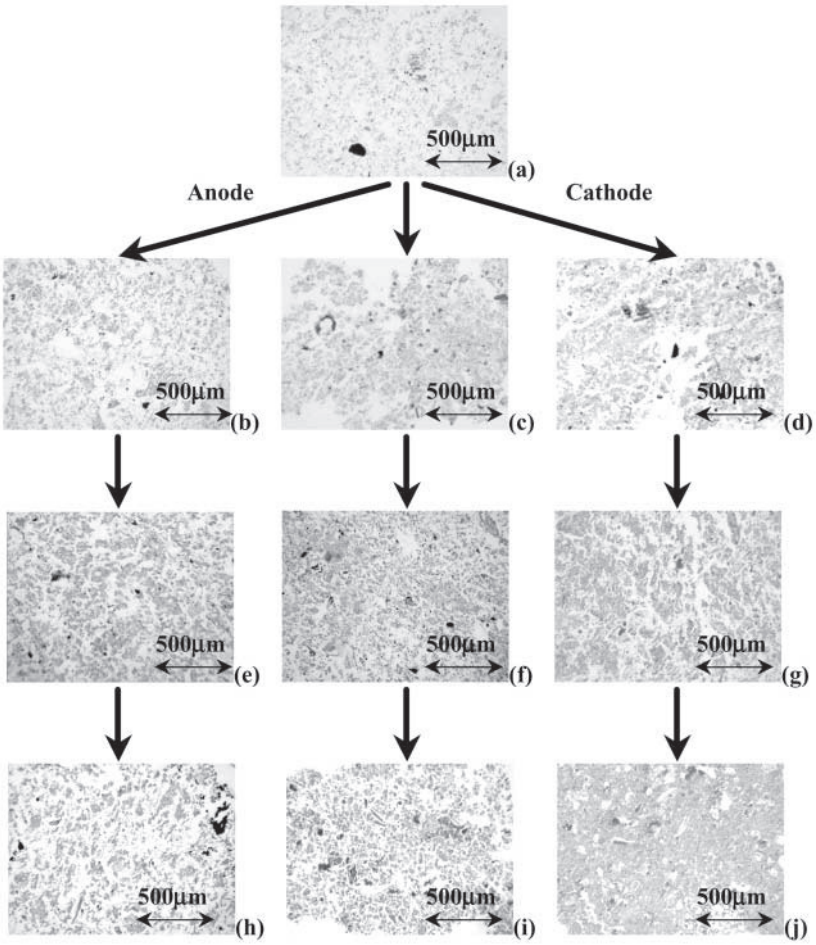

Figure 4. The microtome-sliced images of cakes (40×): (a) suspension; (b) anode, first hour; (c) the middle, first hour; (d) cathode, first hour; (e) anode, second hour; (f) the middle, second hour; (g) cathode, second hour; (h) anode, third hour; (i) the middle, third hour; (j) cathode, third hour.

Porous Configuration

The image analysis was performed to determine the spatial distribution of morphological parameters in the filter. The aforementioned terms such as "porous" or "compact" can thus be quantified. The photographs were

MARCEL DEKKER, INC.
270 Madison Avenue, New York, New York 10016

divided into several ROIs for analysis, and the measured parameters were then averaged. Figure 5 presents the areal porosity ε_{2D}. The error bars of ε_{2D} are quite small, implying that the porosity is generally uniform across each slice (Fig. 5). The gravitationally thickened sludge suspension formed very loose sediment with a porosity of over 0.8. The moisture in these porous spaces is called interstitial water.[15] The dried solid content was measured as 4.19% (w/w), and the moisture content of the biomass granules was about 73%. The moisture herein could be categorized as surface water and chemically bound water, representing 10% of the total volume. The dewatering decreases porosity. Although some data were scattered, the porosity at the cathode was generally lower than that at the anode, and the difference became clear as dewatering proceeded. In the constant-rate period (before 90 min) the difference of porosity between the cathode and anode was insignificant because the water phase was continuously distributed in the pores of sludge. After 90 min, this difference increased. For the cake near the cathode, the sludge clusters were converted into compact forms. However, the sludge clusters near the anode shrunk, leading to larger pores and increased porosity. This is possibly because the saturation of the cake decreased as the electroosmotic dewatering proceeded, as described in the previous paragraph.

Figure 6 presents the pore sizes identified in the slices. The average pore sizes were specified by two parameters, $d_p[4,3]$ and $d_p[3,2]$, determined from

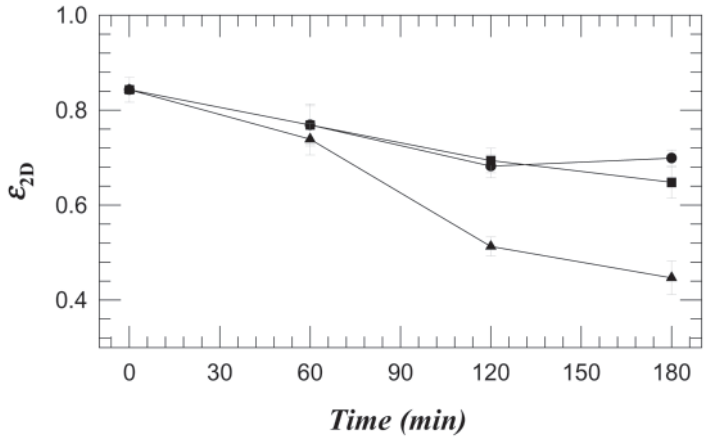

Figure 5. The temporal and spatial evolution of areal porosity ε_{2D}. Circles: anodes; squares: the middle; triangles: cathode.

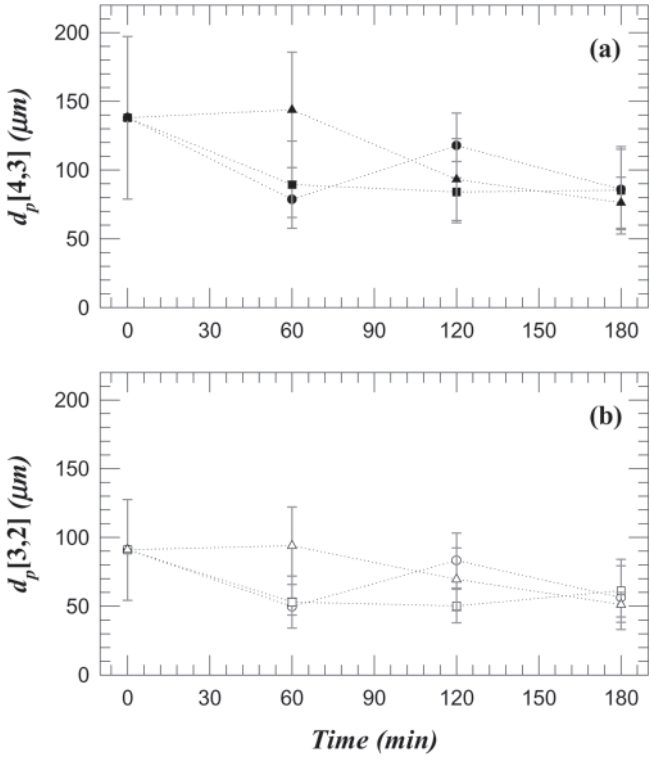

Figure 6. The temporal and spatial evolution of average pore size: (a) $d_p[4,3]$ and (b) $d_p[3,2]$. Circles: anode; squares: the middle; triangles: cathode.

the following definitions,

$$d_p[4,3] = \frac{\sum d_{p,i}^4 n_i}{\sum d_{p,i}^3 n_i} = \frac{\sum d_{p,i} V_i}{\sum V_i} \quad (1)$$

$$d_p[3,2] = \frac{\sum d_{p,i}^3 n_i}{\sum d_{p,i}^2 n_i} = \frac{\sum V_i}{\sum d_{p,i}^{-1} V_i} \quad (2)$$

where $d_{p,i}$, V_i are the diameter and volume of pore i, and n_i is the number of pores of diameter $d_{p,i}$. The large pores in the original sediment disappeared as the moisture was removed. Both sizes had large error bars, indicating that the pore sizes varied greatly at various positions. Roughly, the average pore size shrunk to 60% of the original value in the final stage of dewatering. The variation in pore size at the cathode and in the middle exhibited relatively clear

trends, gradually declining as dewatering proceeded, whereas the size of the pores at the anode fluctuated with time. The decrease in pore size increased the resistance for the fluid passing through and was correlated with the decrease in filtration rate after the 90th minute.

These results in Fig. 6 indicated that the pore size varied greatly at different positions on the slices. Restated, the details of the porous configuration on the slice were highly non-uniform.

Pore Structure

The complex characteristics of cake morphology and pore shapes were quantified using Sierpinski fractal dimensions (D_{SC}) and the fractal dimensions of the pore boundaries (D_B). D_B is used to describe the fractal characteristics of the boundary lines of discrete cake pores. For a pore with rugged boundaries, the following relationship exists between the area and the perimeter,[16]

$$A_p \propto p_p^{2/D_B} \tag{3}$$

where D_B is the fractal dimension of the pore boundaries [Figure 7(a)]. For a circular object, D_B equals one. A rougher and more irregular floc boundary corresponds to a larger D_B value. A_p and p_p in Eq. (3) were determined by applying the maximum convex perimeter method. Restated, once the thresholding value is selected, the total length of the edges of a blob (including the edges of any holes) determines the perimeter of the pore (p_p), and the area of the blob is the pore area (A_p).

Moreover, assuming that the cross section of sludge floc can be described as a Sierpinski carpet, the Sierpinski carpet fractal dimension D_{SC} can be used to quantify the "disappearing rate" of the void area (β^R) of the cross-sectional area when the image resolution is increased and smaller pores can be detected.[16] Figure 7(b) presents one example. β^R is normalized to the total area of the sampling area and is then denoted as β^0. The slope of the curve m represents the rate of disappearance of the "carpet." The curves in regions of high α ($>10\,\mu$m, say) and low α had different slopes, implying that the structure had two levels. Generally, the rate of disappearance decreased on smaller length scales. The Sierpinski fractal dimension, D_{SC}, can be determined by subtracting m from the classical dimension of the surface (two). A lower D_{SC} represents a more compact carpet. The areal porosity (ε_{2D}) was determined by Otsu's method.[17] The distribution of the pore sizes, on the other hand, was determined by applying the maximum convex perimeter method.[13]

Figure 8(a) shows the results. Although the average size varied greatly among different positions (Fig. 6), the error bars on D_B were quite small,

Marcel Dekker, Inc.
270 Madison Avenue, New York, New York 10016

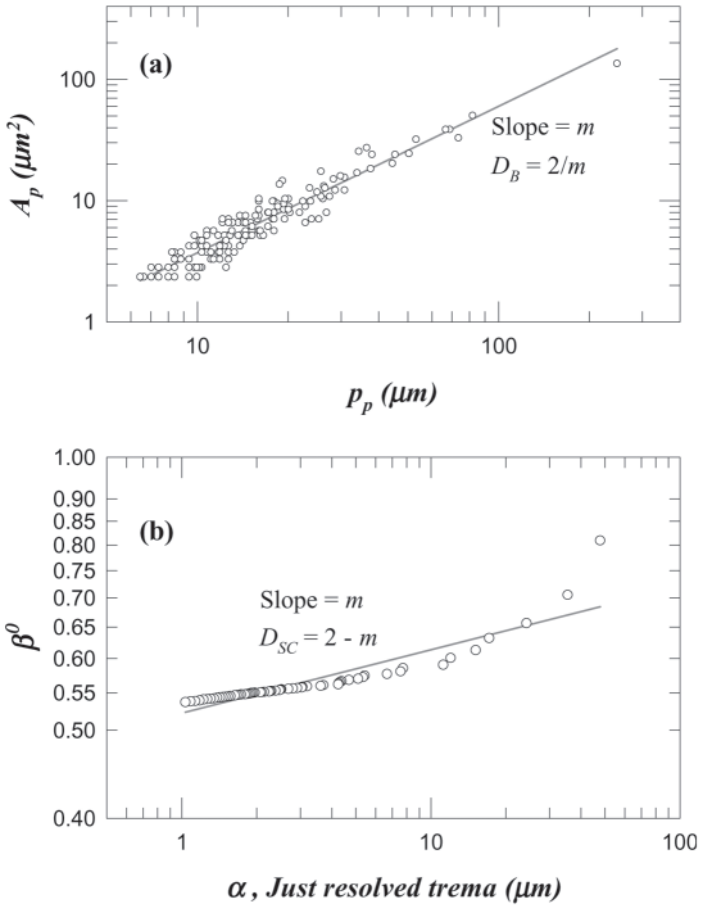

Figure 7. Ways to estimating fractal dimensions: (a) D_B and (b) D_{SC}.

indicating that the pores on the slice exhibited the same fractal characteristics of their boundaries. For the pores at the anode, D_B decreased during the first 2 hr, but significantly increased at the third hour. The pores at the cathode and in the middle exhibited a sharp decrease in D_B after the first hour (from 1.4 to 1.2), implying that the pores became compact and regular and their boundaries became smooth after the constant-rate period had ended.

Figure 8(b) presents resulting values of D_{SC}. The sludge suspension before dewatering had D_{SC} of about 1.60. The entire structure became compact as dewatering continued. The values of D_{SC} ranged from 1.65 to 1.80 at the first hour, increasing to 1.90 for cakes at the second and third

Marcel Dekker, Inc.
270 Madison Avenue, New York, New York 10016

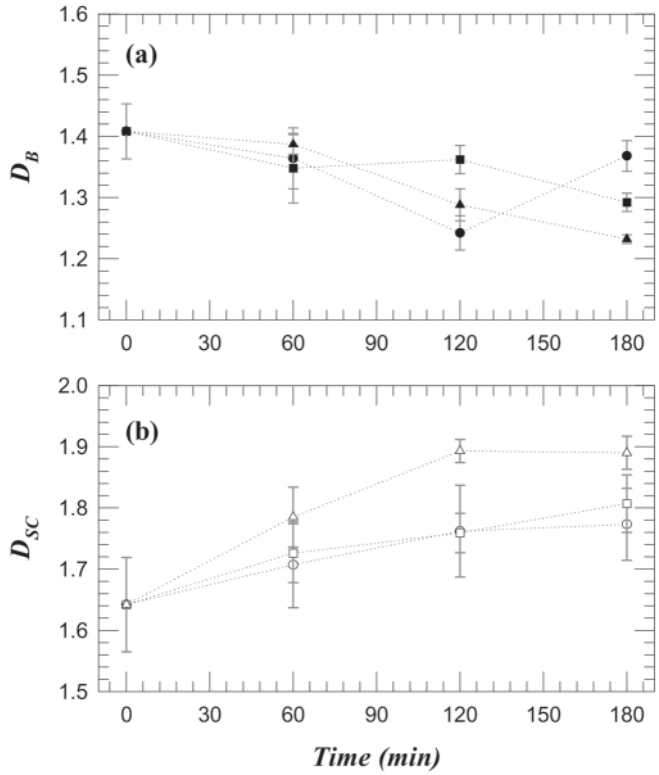

Figure 8. The temporal and spatial distribution of fractal dimension. (a) Boundary fractal dimension D_B; (b) Sierpinski carpet fractal dimension D_{SC}. Circles: anode; squares: the middle; triangles: cathode.

hours. The region near the cathode exhibited a slightly higher D_{SC} during at the zeroth and first hours but almost same during the second and third hours. Restated, the increase in D_{SC} from 1.7 to 1.9 was strongly correlated with the decrease in the dewatering rate (Fig. 3) and a reduction in porosity (Fig. 5).

The aforementioned results suggest a schematic to the structural changes during electroosmosis dewatering of sludge cake. As the dewatering proceeded, the flocs were initially randomly packed on the anode without a compact structure. During the constant-rate period (before the 90th minute), the inter-aggregate and intra-aggregate interstices were filled with water. As the moisture was drained out, the flocs gradually coagulated, the clusters became larger and the pores shrunk. A higher D_B (more than 1.3) implied

more irregular pores, which could retain more interstitial water. When most free moisture had been removed and the rate of dewatering slowly reduced (falling-rate period), the cake saturation decreased, leading to the collapse in the overall porous structure [lower ε_{2D} in Fig. 5 and d_p in Fig. 6(a)]. As the moisture in the cake at the anode was removed and transferred to the cathode, a considerable shrinkage of biomass granules at anode was observed. The compact cake at the cathode retained plenty of surface water, because of continuous replenishment of moisture. The variation in D_{SC} [Fig. 8(b)] and D_B [Fig. 8(a)] reflects the transition in the dewatering rate: a marked change was observed after the constant-rate period has ended.

CONCLUSIONS

Sludge cakes sampled at various positions and times in an electroosmosis dewatering chamber were analyzed by microtome slicing to elucidate the morphological variation. The flocs accumulated at the anode due to the electrostatic attraction. The porosity continued to decrease as most of the biomass coagulated into large clusters. During the constant-rate period, the morphological differences between the cakes at the two electrodes became less significant. During the falling-rate period, a relatively large difference in cake porosity appeared between the electrodes, involving difference in both pore size and porosity. As the moisture in the cake at the anode was removed and transferred to the cathode, a considerable shrinkage of biomass granules at the anode was observed. The compact cake at the cathode retained plenty of surface water, because of continuous replenishment of moisture. The specific surface area did not exhibit a simple trend when the dewatering rate was gradually decreased. The transition in the dewatering rate was also reflected by the Sierpinski fractal dimension (D_{SC}) and pore boundary fractal dimensions (D_B).

APPENDIX: THE OTSU'S METHOD AND THE MAXIMUM CONVEX PERIMETER METHOD

Otsu[17] described a method based on the discriminant analysis. He defined the within-class variance σ_L^2 (or local variance) and the between-class variance σ_J^2 (or joint variance) as follows,

$$\sigma_L^2 = P_0\sigma_0^2 + P_1\sigma_1^2 \tag{A1}$$

$$\sigma_J^2 = P_0(\mu_0 - \mu_T)^2 + P_1(\mu_1 - \mu_T)^2 = P_0(1 - P_0)(\mu_0 - \mu_1)^2 \tag{A2}$$

MARCEL DEKKER, INC.
270 Madison Avenue, New York, New York 10016

Maximizing the between-class variance or minimizing the within-class variance yields the optimal thresholding value i_t. Otsu's method is also equivalent to minimizing the mean square error between the gray-level image and its corresponding bilevel image. Our evaluation shows that Otsu's method yields more stable performance than other histogram-based algorithms and is chosen to obtain the porosity. The frames of the floc matrix on the slices were clearly presented using Otsu's method, and thus gives the estimate of porosity (ε_{2D})

Convex perimeter ($p_{C,p}$) is an approximate of the perimeter of the convex hull of a blob derived from the eight Feret diameters of the blob. The sum of convex perimeters ($\Sigma p_{C,p}$) is maximum at some thresholding value. This method is called "the maximum convex perimeter method" hereafter. Although the small pores occupied an insignificant fraction of the area, they contributed most of the total convex perimeter. As the convex perimeters approached the maximum, small pores (noise) in the images could clearly appear. Therefore, the maximum convex perimeter method can probed the small blobs (pores) among the biomass granules and thus yields the spatial distribution of pores in the floc.

REFERENCES

1. Kondoh, S.; Hiraoka, M. Commercialization of pressurized electroosmotic dehydrator (PED). Wat. Sci. Tech. **1990**, *22* (12), 259–268.
2. Smollen, M.; Kafaar, A. Electroosmotically enhanced sludge dewatering: pilot-plant study. Wat. Sci. Tech. **1994**, *30* (8), 159–168.
3. Barton, W.A.; Miller, S.A.; Veal, C.J. The electrode watering of sewage sludges. Drying Tech. **1999**, *17* (3), 497–522.
4. Buijs, P.J.; Van Diemen, A.J.G.; Stein, H.N. Efficient dewatering of waterworks sludge by electroosmosis. Colloids Surf. A **1994**, *85* (1), 29–36.
5. Snyman, H.G.; Forssman, P.; Kafaar, A.; Smollen, M. Feasibility of electro-osmotic belt filter dewatering technology at pilot scale. Wat. Sci. Tech. **2000**, *41* (8), 137–144.
6. Zhou, J.X.; Liu, Z.; She, P.; Ding, F.X. Water removal from sludge in a horizontal electric field. Drying Tech. **2001**, *19* (3–4), 627–638.
7. Laursen, S.; Birgerjensen, J. Electroosmosis in filter cakes of activated-sludge. Wat. Res. **1993**, *27* (5), 777–783.
8. Yoshida, H. Practical aspects of dewatering enhanced by electro-osmosis. Drying Tech. **1993**, *11* (4), 787–814.
9. Yoshida, H.; Kitajyo, K.; Nakayama, M. Electroosmotic dewatering under A.C. electric field with periodic reversals of electrode polarity. Drying Tech. **1999**, *17* (3), 539–554.

MARCEL DEKKER, INC.
270 Madison Avenue, New York, New York 10016

10. Weber, K.; Stahl, W. Improvement of filtration kinetics by pressure electrofiltration. Sep. Puri. Tech. **2002**, *26* (1), 69–80.
11. Chui, H.K.; Fang, H.H.P. Histological analysis of microstructure of UASB granules. J. Envir. Eng. **1994**, *120* (5), 1322–1326.
12. Carson, F.L. *Histotechnology: A Self-Instructional Text*; ASCP (American Society of Clinical Pathologists) Press: Chicago, USA, 1990; Chapter 3, 43–68.
13. Chu, C.P. A Study on Floc Structure. Ph.D. Dissertation. National Taiwan University: Taipei, Taiwan, 2003.
14. Hamed, J.T.; Bhadra, A. Influence of current density and pH on electrokinetics. J. Haz. Mat. **1997**, *55* (1–3), 279–294.
15. Vesilind, P.A.; Martel, C.J. Freezing of water and wastewater sludges. J. Envir. Eng. **1990**, *116* (5), 854–862.
16. Mandelbrot, B.B. *The Fractal Geometry of Nature*; W.H. Freeman and Co.: New York, USA, 1983.
17. Otsu, N. A threshold selection method from gray-level histogram. IEEE Trans. Syst. Man Cybern. **1979**, *9* (1), 62–66.

Received July 2003
Revised November 2003